scientific reports

Check for updates

OPEN

Symmetry driven altermagnetic spin splitting in hexagonal CrTe from first principles

Rahul Singh[1], Hung-Lung Huang[2], Chih-Huang Lai[1,3] & Horng-Tay Jeng[2,4,5]✉

Altermagnets are a new class of magnetic states that exhibit substantial spin splitting while maintaining zero net magnetization without spin-orbit coupling. CrTe has experimentally been considered an antiferromagnetic (AFM) material. However, in this study, we demonstrate that CrTe exhibits the characteristics of an altermagnet rather than a conventional AFM through first-principles calculations based on density functional theory (DFT). We reveal a collinear magnetic order with significant spin splitting in certain antiferromagnetic configurations. This spin splitting indicates symmetry-protected spin polarization without net magnetization, suggesting that CrTe is a high-potential altermagnet candidate. Our findings contribute to the growing body of research on materials capable of generating spin transport without macroscopic magnetization, thereby providing new opportunities for spintronic applications.

A truly fast-moving field of spintronics is in search of new magnetic phases and functionalities beyond conventional ferromagnetic (FM) and antiferromagnetic (AFM) materials. New magnetic materials have been proposed under the term "altermagnet", which essentially exhibit alternating spin polarization with a strong spin-split band structure, as in ferromagnets, while resulting in zero net macroscopic magnetization, as in antiferromagnets[1,2]. Altermagnetism occurs because of symmetry breaking in the magnetic lattice with spin-dependent electron hopping, causing significant spin splitting and intermediate transport without the assistance of any external magnetic fields[2,3]. These unique properties make altermagnets prime candidates for next-generation spintronic devices using spin currents and spin-orbit torque, while evading the limitations imposed by stray fields and domain instability in ferromagnets[4,5].

Recent attempts have been made to identify materials as altermagnet candidates. One of the earlier proposed altermagnets is CrSb, which exhibits spin-split electronic structures and non-collinear spin configurations, thus breaking time-reversal symmetry (TRS) without creating any net magnetization[6–12]. Similarly, MnTe exhibits strong spin-polarized transport, with the spin splitting predicted to increase under doping or perturbation, thus underscoring its potential in spintronic applications[12–18]. RuO_2 was believed to be paramagnetic until recently, when it was identified as an altermagnet owing to spin-polarized transport and significant anomalous Hall effects (AHE) introduced by symmetry-protected spin splitting[19–23].

Chromium telluride (CrTe) stands out among candidate altermagnetic materials due to its intricate magnetic phase diagram and tunable electronic structure[24–26]. CrTe is known to exhibit complex temperature-dependent magnetism in both bulk and thin-film forms: it is paramagnetic above 330 K, ferromagnetic between 110 K and 330 K, and antiferromagnetic below 110 K[26–30]. Although a recent study has explored the surface-oriented altermagnetic states of CrTe[31], a comprehensive understanding of the intrinsic bulk properties specifically the microscopic orbital mechanisms and momentum-dependent spin transport remains lacking. Establishing this bulk physical baseline is essential for fully exploiting the material's potential in spintronics. The interplay between these magnetic phases, lattice symmetry, and electron correlations renders CrTe a promising candidate for realizing robust altermagnetism.

In this study, we present a comprehensive first-principles investigation of the electronic and magnetic properties of hexagonal CrTe using density functional theory (DFT). Our spin-resolved band structure calculations reveal pronounced spin splitting and spin polarization without net magnetization in the antiferromagnetic configuration, providing direct evidence for symmetry-protected collinear altermagnetism.

[1]College of Semiconductor Research, National Tsing Hua University, Hsinchu 30013, Taiwan. [2]Department of Physics, National Tsing Hua University, Hsinchu 30013, Taiwan. [3]Department of Materials Science and Engineering, National Tsing Hua University, Hsinchu 30013, Taiwan. [4]Physics Division, National Center for Theoretical Sciences, Taipei 10617, Taiwan. [5]Institute of Physics, Academia Sinica, Taipei 11529, Taiwan. ✉email: jeng@phys.nthu.edu.tw

Furthermore, we clarify the orbital origins of this splitting and analyze the bulk Fermi surface topology. This combination of zero net magnetization and symmetry-driven spin splitting opens innovative routes for efficient spin current generation and manipulation, significantly expanding the material landscape for future spintronic technologies.

First-principles electronic structure calculations based on density-functional theory with the generalized gradient approximation (GGA) parameterized by Perdew–Burke–Ernzerhof (PBE)[32–34] for exchange-correlation interactions were performed for CrTe using the Vienna Ab initio Simulation Package (VASP)[35]. CrTe crystallizes in a NiAs-type structure with hexagonal symmetry (space group $P6_3/mmc$, No. 194). A plane-wave energy cutoff of 500 eV and a 6 × 6 × 5 Gamma-centered Monkhorst-Pack k-point mesh over the hexagonal Brillouin zone (BZ) were used to ensure accurate convergence of the total energies and electronic properties. The valence electron configurations considered in the pseudopotentials were Cr ($3d^5 4s^1$) and Te ($5s^2 5p^4$). Structural optimizations were carried out using the PBE + U method with U_{eff} = 3.5 eV[36] for Cr and 0.0 for Te until the forces on atoms were less than 0.001 eV/Å. The fully relaxed lattice parameters were a = 4.259 Å, b = 4.259 Å, and c = 6.288 Å. Self-consistent field calculations were performed until the total energy differences between subsequent steps were less than 10^{-6} eV. The VASPKIT was used for the post-processing of the output data from VASP[37]. For the spin polarization calculation in Fig. 5(b), we took the integration density of states (iDOS) around the fermi-level from − 0.2 eV to 0.2 eV at hundred discrete points along the k-path using the formula:

$$Polarization = \frac{iDOS\,(up) - iDOS\,(down)}{iDOS\,(up) + iDOS\,(down)}.$$

Several metallic altermagnetic candidates have been reported, namely, CrSb, $CrNb_4S_8$, and RuO_2[38]. Herein, we report CrTe as another metallic altermagnet candidate with a large band splitting near the Fermi level. Previously, CrTe was reported to show antiferromagnetic properties at temperatures below 110 K[30]. However, our investigations using first-principles calculations without spin-orbit coupling demonstrate large spin-split bands with spin-split bands flipping symmetrically about the nodal points. Figure 1 presents the atomic structure and location of the spin-split points of CrTe in the Brillouin zone. Figure 1a shows the top view of the unit cell with the Cr and Te atomic positions emphasized. Figure 1b shows a side view of the structure with the magnetic moments of the Cr atoms oriented antiparallel to the crystal c-axis. This type of spin arrangement results in a local symmetry, where the spin orientations alternate in the material. Figure 1c depicts the k-path L'-G-L in the Brillouin zone with spin-split bands for the observed altermagnetism. Significant spin splitting has been previously reported for CrSb and MnTe[39]. Figure 1d shows the electronic band structure of CrTe along the path L'–G–L with the symmetry points defined in fractional reciprocal lattice coordinates as L' at (-0.5, 0, 0.5), G at (0, 0, 0), and L at (0.5,0, 0.5). The symmetry equivalence of this path is presented in Supplementary Information (SI) Sect. 2. The path extends from L' to L through the bulk Brillouin zone center (G). This trajectory allows for the examination of the momentum-dependent spin splitting and its sign reversal across the zone center. The symmetry operation responsible for altermagnetic splitting along the path L'-G-L is demonstrated in SI as well. The splitting magnitude for CrSb and MnTe are 1200 and 1100 meV, respectively, reported previously[39]. Here, we observe a considerable spin splitting of about 1066 meV similar to that in CrSb and MnTe near the Fermi level along the L'–G–L path. In addition, we show variation of spin-splitting magnitude with strain in SI Fig. 7(d). Moreover, the spin bands are flip-symmetric with respect to the nodal point G, an aspect shared with the symmetry-driven spin polarization in known altermagnets. Hence, this feature of spin splitting and symmetry about the nodal point serves as a compelling argument for regarding CrTe as an altermagnetic candidate.

Figure 2a shows the total density of states (TDOS) for the altermagnetic state of CrTe, with the Fermi level located at zero energy. The symmetric DOS in the spin-up and spin-down channels displays a zero net magnetic moment despite the spin-split bands shown in Fig. 2c. The spin band splitting in the absence of net magnetization in altermagnets arises from the broken Kramers Degeneracy without spin-orbit coupling in a collinear magnetic

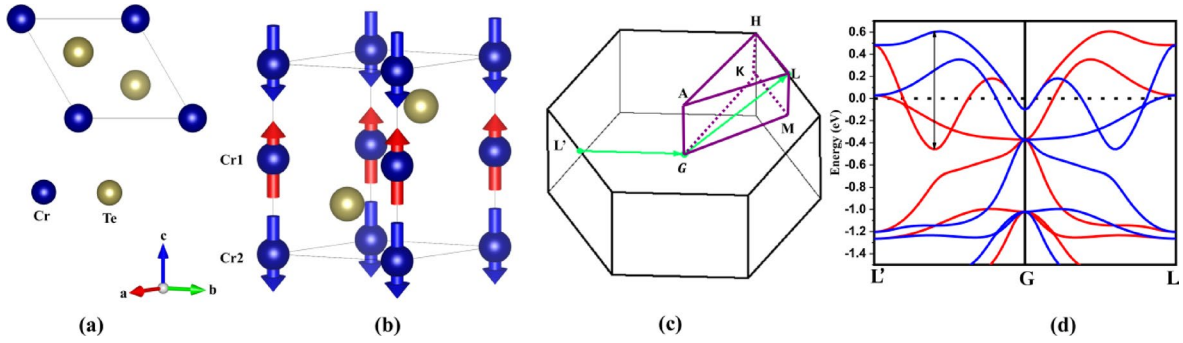

Fig. 1. (**a**) and (**b**) show top and side views of the CrTe crystal structure, respectively. The magnetic structure is shown in the side view, with red and blue arrows indicating spin-up and spin-down, respectively. (**c**) The green line L'-G-L indicates the band structure path in the Brillouin zone, with spin-split bands illustrated by the red and blue bands in the inset. The dotted horizontal line in the inset represents the Fermi level. (**d**) Spin-decomposed band structures for CrTe using PBE without SOC. The red and blue bands represent the spin-up and spin-down states, respectively. The black arrows indicate the maximum spin splitting.

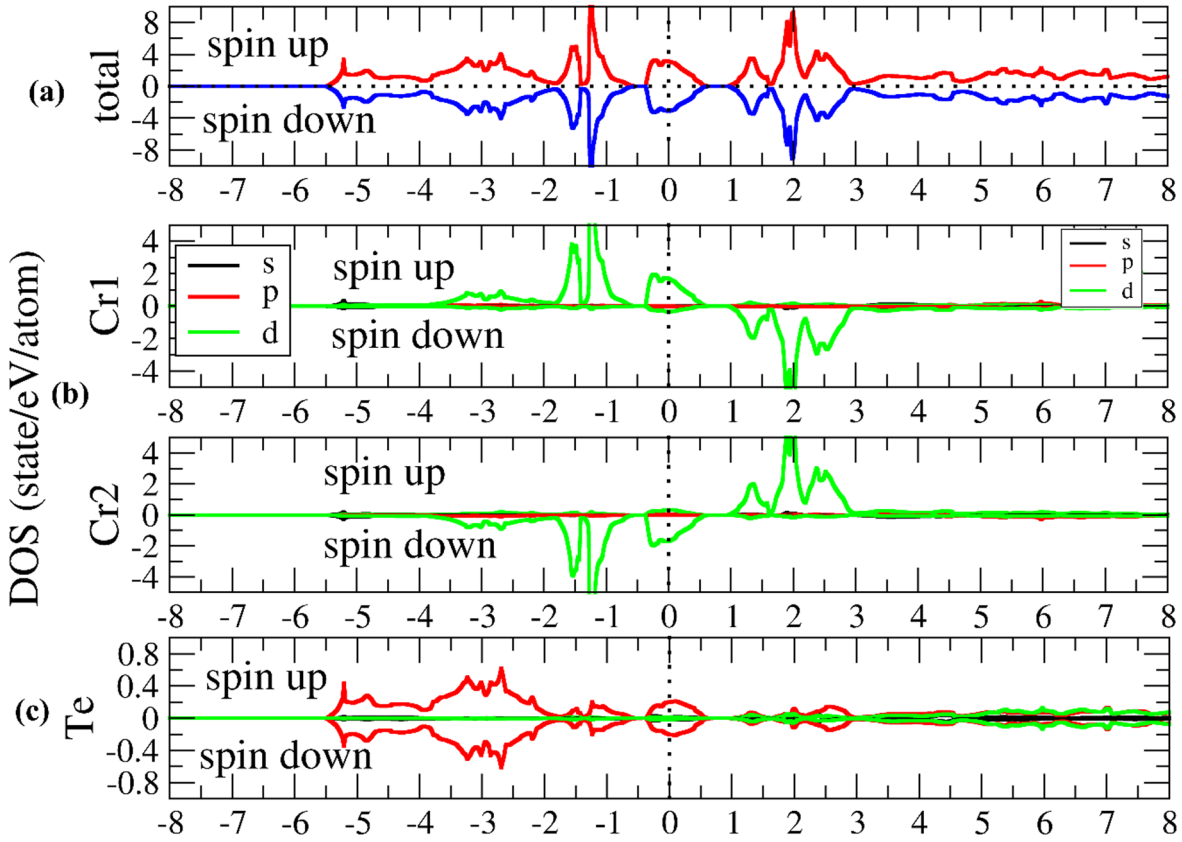

Fig. 2. (**a**) Total density of states (DOS) of CrTe calculated using PBE. (**b**) Orbital-resolved PDOS of Cr (Cr1 and Cr2 for spin-up and spin-down atoms, respectively). (**c**) Orbital-resolved PDOS of Te.

structure and does not produce macroscopic magnetization[14]. The features appearing in this DOS strengthen the claim that CrTe is an altermagnet, in agreement with the results from the band structure.

Moreover, in the energy window from − 1.5 eV to 0.5 eV around the Fermi energy, the PDOS of Cr atoms (Fig. 2b) shows that the dominant contributions arise from the d-orbitals. Both spin-up and spin-down atoms exhibit a strong d-orbital weight concentrated just below and slightly above the Fermi level. This region is critical for electronic transport and spin polarization, making d-state dominance a key feature in the emergence of spin-split bands. Thus, with a greater contribution from the Cr d-states than from the s- and p-states, it is clear that these are the states on which the magnetic and conducting properties of CrTe are built. This is consistent with the general behavior exhibited by transition metals in the case of chalcogenides, where partially filled d-orbitals mediate magnetic exchange interactions and build up the bands. The pronounced spin symmetry between the spin-up and spin-down states in this energy window reiterates the collinear antiferromagnetic ordering with significant spin splitting. Figure 2c shows the projected density of states of Te in CrTe. The Te-5p orbitals make a major contribution to the energy window from − 1.5 to 0.5 eV with respect to the Fermi level.

In Fig. 3a–h, we show spin and orbital projected spectral-weight band structure calculations from 1.5 eV below to 0.5 eV above the Fermi level. The orbital dependent spin polarization can be seen clearly through the color brightness. Cr d-orbitals have major contributions to the spin splitting bands with minor contributions from s- and p-orbitals (less than 0.2). This orbital-resolved nature of the spin asymmetry forms the basis of the altermagnetic character of CrTe and its usefulness for spintronic applications. In Fig. 3i–l, the spectral weight also presents the greatest components of the spin splitting bands are from the Te-5p orbitals, which confirms their participation in the low-energy electronic structure and their strong hybridization with the Cr-3d orbitals. The Te-d and s orbitals contribute only slightly (the weightage is below 0.2). This suggests their lesser influence on magnetic interactions. Although the contribution of Te is almost half that of Cr, the spectral weight confirms the nontrivial attribution of the Te-p states to the spin-split features and magnetic interactions in CrTe.

Figure 4a presents the k-resolved spin density by integrating the occupied spin-polarized DOS at each k-point along the L'–G–L path. The spin density is mainly contributed by the magnetic Cr d-orbitals. Positive values correspond to higher spin-up occupations, whereas negative values represent higher spin-down occupations at each k-point. A clear antisymmetric distribution of the k-dependent spin density about the G point was observed. Specifically, bands that exhibit a spin-up character in the L' to G segment are mirrored by bands with a spin-down character in the G to L segment. This pattern is consistent with the flip symmetry previously described in Fig. 1d, where the spin-resolved bands exhibit no net magnetization (NM).

Figure 4b displays the spin polarization around the Fermi level from − 0.2 eV to 0.2 eV by integrating the difference between the spin-polarized DOS within this energy window to mimic the k-dependent spin-polarized

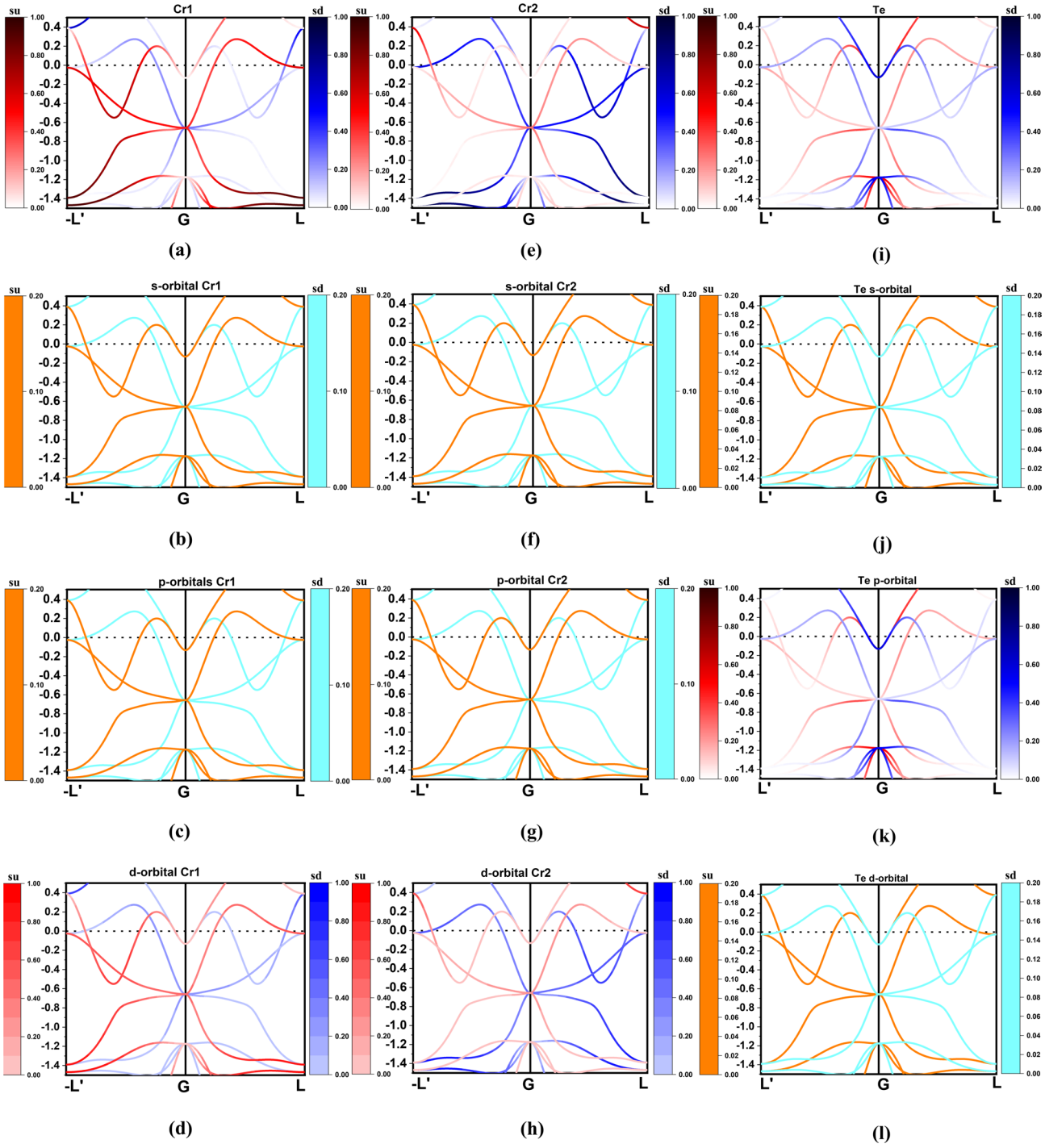

Fig. 3. Spin and orbital decomposed band structure of altermagnet CrTe. (**a**–**h**) for Cr and (**i**–**l**) for Te. In legend: su is for spin up and sd for spin down in their respective orbital. The color scale depicts the spectral weight using PBE without SOC.

transport behavior along the high-symmetry L'–G–L path. Along the GL' direction, carriers display slight spin-down polarization for low wave vectors (low-k) and strong spin-up polarization for middle and high wave vectors (high-k). In contrast, this k-dependent spin polarization behavior is reversed along the GL direction. Such novel transport behavior could be used in future spintronics applications for spin-selected nanodevices. The spin-up and spin-down bands exhibit mirror symmetry about the G point, indicating that the spin polarization is anti-symmetrically distributed along L' to G and G to L respectively. This anti-symmetric spin texture is a hallmark of altermagnetic band splitting and is corroborated by the spin-resolved band structure in Fig. 1d, where the spin-split bands are inverted across the G point. Such behavior reinforces the classification of CrTe as an altermagnet with momentum-dependent spin polarization and vanishing net magnetization[40,41].

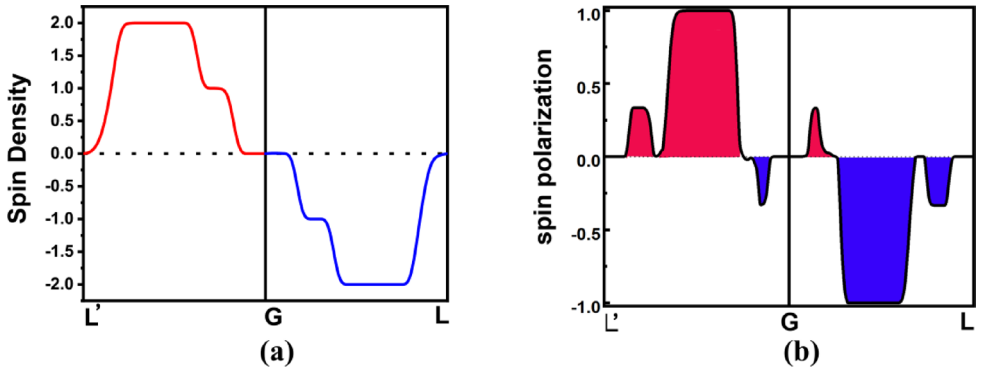

Fig. 4. Spin density and spin polarization around the Fermi level (-0.2 ~ 0.2 eV) along the k-path: L', G, and L for CrTe, using PBE.

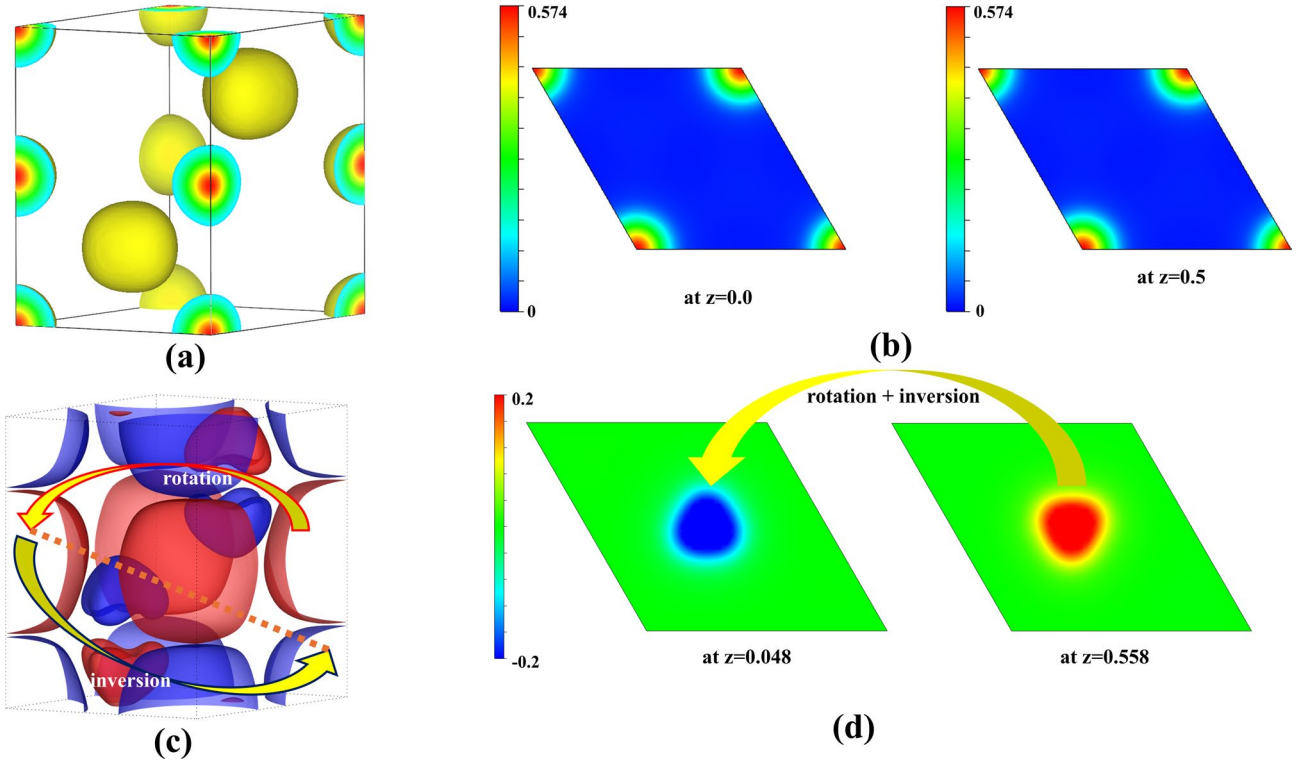

Fig. 5. (**a**) 3D charge density contour of CrTe. (**b**) 2D charge density distribution in the (001) plane at z = 0.0 and z = 0.5. (**c**) 3D isosurface of spin density contour. (**d**) Spin density at z = 0.048 and 0.558, the x-y boundary is shifted to -0.5 ~ 0.5 along a-b for clarity. The yellow arrows in (**c**) and (**d**) indicate the roto-inversion symmetry of altermagnetism in CrTe. The spin density distribution changes sign under the roto-inversion operations. Unit of color-bar: electrons per cubic angstrom (e/Å^3). All calculations are calculated using PBE.

Figure 5a shows the 3D electron density distribution centered on the Cr and Te atoms. Cr exhibits a high charge density with a localized character, whereas Te shows a lower charge density distributed diffusively. Figure 5b depicts the 2D electron density distributions in the (001) plane at z = 0.0 and z = 0.5 for Cr atoms. In contrast, the 3D and 2D spin density distributions in Fig. 5c,d illustrate the isosurface which shows the real-space spin density with pronounced tri-lobed d-like polarization on the transition-metal sites. Neighboring layer Cr ions carry opposite sign of spin density with a rotated lobe orientation, directly visualizing the two symmetry-related sublattices. The anisotropy of spin density at z = 0.048 and 0.558 visualizes as complementary triangular and reverse-triangular patterns on the two magnetic sublattices, provides a direct structural fingerprint of the defining roto-inversion symmetry of the altermagnetic phase. This observation directly bridges the crystallographic symmetry with the electronic structure: the anisotropic local environment is the origin of the anisotropic exchange interactions that, in turn, produce the hallmark momentum-dependent spin splitting in the Brillouin zone[2,39–43] as shown in Fig. 1d. The real-space imaging of this sublattice-specific spin density

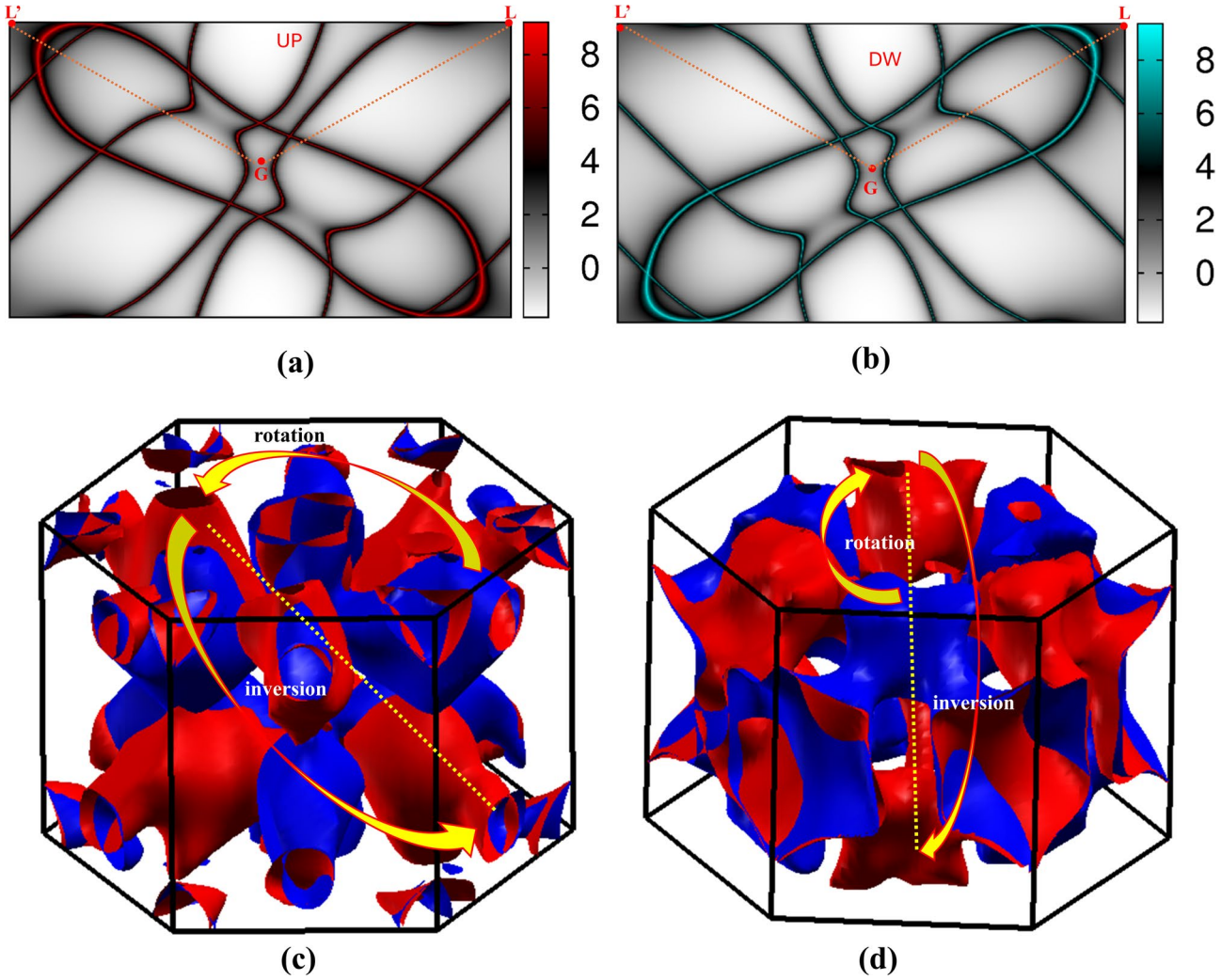

Fig. 6. (**a**,**b**) 2D sliced fermi surface for spin up and spin down respectively, along L'GL. The color scale shows the k-resolved spectral weight A(k, E_F) (Arbitrary Units) on a logarithmic scale. (**c**,**d**) 3D fermi surface of spin band number 12,13 showing roto-inversion, red for spin-up and blue for spin-down, calculated using PBE without SOC.

anisotropy serves as a crucial experimental counterpart to the k-space signature of altermagnets, confirming the direct-to-reciprocal-space correspondence that underpins this distinct magnetic phase and its unconventional g-wave altermagnetism. In addition to the spin-split bands in reciprocal space (Fig. 1d), these results clearly demonstrate the altermagnetism in CrTe.

The spin-polarized Fermi surface (FS) without SOC is presented in Fig. 6a, b. A direct correlation with the spin-splitting band structure in Fig. 1d is evident: along the high-symmetry direction L'–G, the Fermi level is crossed four times by spin-up bands and twice by spin-down bands, a pattern that is precisely inverted along the G–L direction. We observe a clear g-wave–like spin texture in Figs. 6(c, d), in agreement with the symmetry-based expectation for altermagnets belonging to the 6/mmm class and consistent with theoretical predictions that g-wave altermagnets host a g-wave–symmetric Fermi surface[2,44] and analogous to previous reports for CrSb and MnTe[2]. This robust, momentum-dependent spin texture of the Fermi surface, calculated without SOC, is a hallmark signature of altermagnetism, recently confirmed in CrSb by spin-resolved ARPES to reach energies up to ~ 1.0 eV near the Fermi level[7]. The clear alternation of dominant spin character along orthogonal crystal directions, directly linked to the asymmetric band crossings, demonstrates the key altermagnetic trait of strong time-reversal symmetry breaking without a net magnetic moment[39]. For comparison, Fig. 9 in SI shows Fermi surface calculated with SOC. Furthermore, such spin splitting is foundational to the emergence of non-trivial topology in altermagnets, as demonstrated by the observation of spin-polarized Fermi arcs arising from altermagnetic Weyl nodes in CrSb[45].

Finally, some detailed electronic structures of CrTe are provided in SI Information (SI). SI Fig. 1 in the SI shows the spin-resolved band structures along the standard k-path in the hexagonal BZ. All the spin-up and spin-down bands coincided with each other, showing no spin splitting along these high-symmetry paths. Figure 2 in SI compares the spin resolved band structures with and without on-site Hubbard U. SI Fig. 3 shows the

U-dependent band structures. Both show clear altermagnetism in CrTe, demonstrating the robust altermagnetic spin polarized bands against the strong correlation. Figure 4 in SI presents comparison on partial density of states with and without U. Both show no net magnetic moments as expected for altermagnetism. SI Fig. 5 present Cr-s, p, d atomic orbital decomposition spin polarized band structure without spin-orbit coupling. Figure 6 in SI shows the altermagnetic spin splitting band structure with spin-orbit coupling included. In SI Fig. 7, we further show that altermagnetic spin splitting is still valid on applying strain. Figure 8 shows U-dependent spin polarized band structures with the magnetic moment along [001], [010] and [001] directions. Clearly the altermagnetic spin splitting band structure is robust against spin-orbit coupling, magnetic anisotropy, and strain. Whereas SOC + U calculations (SI Table 1) yield a small, tunable magnetocrystalline anisotropy for switching the easy axis between in-plane and out-of-plane at moderate U_{eff}. SI Fig. 9 illustrate the 2D and 3D altermagnetic Fermi surfaces with spin-orbit coupling included. At the end of SI, BZ symmetry analysis are presented.

In conclusion, our first-principles study demonstrates that CrTe, which has long been considered an antiferromagnetic (AFM) material, but exhibits altermagnetism. This is characterized by spin-split electron bands within a collinear antiferromagnetic structure, but crucially, with zero net magnetization. Through first-principles calculations based on DFT, we reveal substantial spin splitting along the symmetry path L'–G–L in the Brillouin zone, further confirming that CrTe does not exhibit any macroscopic magnetization—an essential hallmark of altermagnets. The spin-up and spin-down bands are mirror images of each other and spin-flip around the G point, consistent with the defining signatures of altermagnets. Analysis of the partial density of states (PDOS) and spectral weight reveals that the spin-polarized states near the Fermi level are primarily composed of Cr-3d with minor component of Te-5p orbitals. CrTe remains metallic in the altermagnetic phase with a k-dependent spin polarized density of states at the Fermi level, suggesting that this material is well-suited for spintronic applications such as spin-selected transport devices. These insights not only underscore its potential but also lay the foundation for future innovations in spintronic technologies that exploit spin polarization without the constraints of macroscopic magnetization.

Data availability

The data which show our result are available from the authors upon reasonable request.

Received: 16 December 2025; Accepted: 30 January 2026
Published online: 27 March 2026

References

1. Šmejkal, L. et al. Giant and tunneling magnetoresistance in unconventional collinear antiferromagnets with nonrelativistic Spin-Momentum coupling phys. *Rev. X*. **12**, 011028 (2022).
2. Šmejkal, L. et al. Beyond conventional ferromagnetism and antiferromagnetism: A phase with nonrelativistic spin and crystal rotation symmetry. *Phys. Rev. X* **12**, 031042.
3. Chao-Chun et al. Crystal chemistry and design principles of altermagnets. *ACS Org. Inorg. Au*. **4** (6), 604–619. https://doi.org/10.1021/acsorginorgau.4c00064 (2024).
4. Benedetta, F. et al. The 2024 magnonics roadmap. *J. Phys. Condens. Matter* **36** (2024).
5. Hongyu et al. Emerging antiferromagnets for spintronics. *Adv. Mater.* **36**, 2310379 (2024).
6. Reimers, S. et al. Direct observation of altermagnetic band splitting in CrSb thin films. *Nat. Commun.* **15**, 2116. https://doi.org/10.1038/s41467-024-46476-5 (2024).
7. Yang, G. et al. Three-dimensional mapping of the altermagnetic spin splitting in CrSb. *Nat. Commun.* **16**, 1442. https://doi.org/10.1038/s41467-025-56647-7 (2025).
8. Zhou, Z. et al. Manipulation of the altermagnetic order in CrSb via crystal symmetry. *Nature* **638**, 645–650. https://doi.org/10.1038/s41586-024-08436-3 (2025).
9. Takahiro et al. High mobility charge transport in a multicarrier altermagnet CrSb. *Phys. Rev. Mater.* **8**, 084412 .
10. Yuqing et al. Nonlinear field dependence of hall effect and high-mobility multi-carrier transport in an altermagnet CrSb. *Appl. Phys. Lett.* **126**, 042402 (2025).
11. Jianyang et al. Large band splitting in 쫘-Wave altermagnet CrSb. *Rev. Lett.* **133**, 206401 (2024).
12. Yu, T. et al. Néel vector-dependent anomalous transport in altermagnetic metal CrSb. *Npj Quantum Mater.* **10**, 47. https://doi.org/10.1038/s41535-025-00766-3 (2025).
13. Orlova, N. N. et al. Crossover from relativistic to Non-Relativistic net magnetization for MnTe altermagnet candidate. *Jetp Lett.* **120**, 360–366. https://doi.org/10.1134/S0021364024602926 (2024).
14. Suyoung et al. Broken Kramers Degeneracy in Altermagnetic MnTe. https://doi.org/10.1103/PhysRevLett.132.036702.
15. Aoyama, T., & Ohgushi, K. Piezomagnetic properties in altermagnetic MnTe. https://doi.org/10.1103/PhysRevMaterials.8.L041402.
16. Osumi, T. et al. Observation of a giant band splitting in altermagnetic MnTe. *Phys. Rev. B*. **109**, 115102 (2024).
17. Krempaský, J. et al. Altermagnetic lifting of Kramers spin degeneracy. *Nature* **626**, 517–522. https://doi.org/10.1038/s41586-023-06907-7 (2024).
18. Nayana et al. Interplay of altermagnetism and pressure in hexagonal and orthorhombic MnTe. *Phys. Rev. Mater.* **8**, 104407 (2024).
19. Olena et al. Observation of time-reversal symmetry breaking in the band structure of altermagnetic RuO2. *Science* **10**, eadj4883. https://doi.org/10.1126/sciadv.adj4883 (2024).
20. Yaqin et al. Direct and inverse spin splitting effects in altermagnetic RuO2. *Adv. Sci.* https://doi.org/10.1002/advs.202400967.
21. Song, J. et al. Spin-Orbit coupling driven magnetic response in altermagnetic RuO2. https://doi.org/10.1002/smll.202407722.
22. Hongyu et al. Spin-Splitting magnetoresistance in altermagnetic RuO2 thin films. *Adv. Mater.* https://doi.org/10.1002/adma.202507764.
23. Noh, S. et al. Tunneling magnetoresistance in altermagnetic RuO2-Based magnetic tunnel junctions. *Phys. Rev. Lett.* **134**, 246703 (2025).
24. Yang, J. et al. Magnetism of two-dimensional chromium tellurides. iScience **26**, 106567 (2023).
25. Jun et al. Structure dependent and strain tunable magnetic ordering in ultrathin chromium telluride. *J. Alloys Compd.* **893**, 0925–8388 (2022).
26. Wang, M. S. et al. Two-dimensional ferromagnetism in CrTe flakes down to atomically thin layers nanoscale **12**, 16427 (2020).
27. He, Y. K. et al. Easy-cone magnetic structure in $(Cr_{0.9}B_{0.1})$Te. *Appl. Phys. Lett.* **116**, 102404 (2020).
28. Wu, H. et al. Strong intrinsic room-temperature ferromagnetism in freestanding non-van der Waals ultrathin 2D crystals. *Nat. Commun.* **12**, 5688. https://doi.org/10.1038/s41467-021-26009-0 (2021).

29. Gao, Z. et al. Near room-temperature ferromagnetism in air-stable two-dimensional $Cr_{1-x}Te$ grown by chemical vapor deposition. *Nano Res.* **15**, 3763–3769. https://doi.org/10.1007/s12274-021-3909-7 (2022).
30. Fu-Sheng, L. et al. Electronic transport and magnetic properties of CrTe epitaxial thin films with room temperature ferromagnetism, surfaces and interfaces, **57**, 105779, ISSN 2468 – 0230. https://doi.org/10.1016/j.surfin.2025.105779 (2025).
31. Apeksha Gauswami & Prafulla, K. J. *J. Phys. : Condens. Matter* **37** 305801 (2025).
32. Perdew, J. P., Burke, K., Wang, Yue & and, Generalized gradient approximation for the exchange-correlation hole of a many-electron system. *Phys. Rev. B*. **54**, 16533 (1996). – Published 15 December.
33. Ochil, P. E. Projector augmented-wave method. *Phys. Rev. B.* **50**, 17953 (1994). – Published 15 December.
34. Perdew, J. P., Burke, K. & Ernzerhof, M. Generalized gradient approximation made simple. *Phys. Rev. Lett.* **77**, 3865 (1996).
35. Kresse, G. & Furthmüller Efficient iterative schemes for Ab initio total-energy calculations using a plane-wave basis set. *Phys. Rev. B*. **54**, 11169 (1996).
36. Lauer, D. et al. Optimizing Hubbard U parameters for enhanced description of electronic and magnetic properties in CrI_3 monolayers and bilayers. *Sci. Rep.* **15**, 18126. https://doi.org/10.1038/s41598-025-01814-5 (2025).
37. Wang, V., Xu, N., Liu, J. C., Tang, G. & Geng, W. T. VASPKIT: A User-Friendly interface facilitating High-Throughput computing and analysis using VASP code. *Comput. Phys. Commun.* **267**, 108033. https://doi.org/10.1016/j.cpc.2021.108033 (2021).
38. Guo, Y. et al. A large-scale ab-initio study. *Mater. Today Phys.* **32**, 100991. https://doi.org/10.1016/j.mtphys.2023.100991 (2023).
39. Libor Šmejkal, J., Sinova & Jungwirth, T. Emerging research landscape of altermagnetism. *Phys. Rev. X*. **12**, 040501 (2022).
40. Cheong, S. W. & Huang, F. T. Altermagnetism classification. *Npj Quantum Mater.* **10**, 38. https://doi.org/10.1038/s41535-025-00756-5 (2025).
41. Mazin, I. & The PRX Editors Editorial. Altermagnetism—A new punch line of fundamental magnetism. *Phys. Rev. X*. **12**, 040002 (2022).
42. Tamang, R., Gurung, S., Rai, D. P., Brahimi, S. & Lounis, S. Altermagnetism and altermagnets: A brief review. *Magnetism* **5**, 17. https://doi.org/10.3390/magnetism503001 (2025).
43. Jungwirth, T. et al. Altermagnetism: An unconventional spin-ordered phase of matter. *Newton* **1**(6), 100162.
44. Motohiko & Ezawa Third-order and fifth-order nonlinear spin-current generation in g-wave and i-wave altermagnets and perfectly nonreciprocal spin current in f -wave magnets. https://doi.org/10.1103/PhysRevB.111.125420.
45. Li, C. et al. Topological Weyl altermagnetism in CrSb. *Commun. Phys.* **8**, 311. https://doi.org/10.1038/s42005-025-02232-9 (2025).

Acknowledgements

H.-T. J. also thanks support from NCHC, CINC-NTU, AS-iMATE-111-12, and CQT-NTHU-MOE, Taiwan.**Author contributions**.

Rahul Singh performed DFT calculations and wrote the original draft. Hung-Lung Huang provided technical supports. Chih-Huang Lai and Horng-Tay Jeng supervised the project. All authors co-wrote and commented on the manuscript.

Author contributions

R.S. performed DFT calculations and wrote the original draft. H.L.H. provided technical supports. C.H.L. and H.T.J. supervised the project. All authors cowrote and commented on the manuscript.

Funding

This work was supported by the National Science and Technology Council, Taiwan.

Declarations

Competing interests

The authors declare no competing interests.

Additional information

Supplementary Information The online version contains supplementary material available at https://doi.org/10.1038/s41598-026-38641-1.

Correspondence and requests for materials should be addressed to H.-T.J.